Available online at www.sciencedirect.com
SCIENCE DIRECT
Polymer 46 (2005) 7018–7027
polymer
www.elsevier.com/locate/polymer

Organic–inorganic nanocomposites from cubic silsesquioxane epoxides: direct characterization of interphase, and thermomechanical properties

Junchao Huang*, Chaobin He, Xueming Liu, Jianwei Xu, Christine S.S. Tay, Shue Y. Chow

Institute of Materials Research and Engineering, 3 Research Link, Singapore 117602, Singapore

Received 31 March 2005; received in revised form 18 May 2005; accepted 22 May 2005
Available online 21 June 2005

Abstract

Novel organic–inorganic nanocomposites were prepared by in situ curing of poly(amic acid) macromolecules with POSS epoxide, octa(ethylcyclohexylepoxidedimethylsiloxy) silsesquioxane (OC). Solid-state ^{29}Si NMR data show that properties of the interphase can be varied systemically by adjusting the nano-tether structure of the POSS molecules. DMA studies conclude that the cross-linking densities of the nanocomposites increase significantly so that some of these nancomposites are found to lose glass transition temperature; the nanocomposite networks were predominantly formed by the linkage between the terminal amine groups of the polyimide molecules and the epoxide groups of the POSS molecules. Furthermore, in the nanocomposites two factors, the soft interphase around OC molecules and the increasing cross-linking density, compete with each other, and their influences on morphologies, coefficient of thermal expansion, mechanical strength and hardness of these nanocomposites were also investigated.

Keywords: Polymer composites; Epoxide; Silsesquioxane

1. Introduction

Copolymers containing inorganic polyhedral oligomeric silsesquioxane (POSS) represent a novel series of nanoscale-structured materials [1–5]. POSS has recently attracted enormous interest and found widespread application in high-temperature and fire-resistance materials [6,7]. The use of POSS nanoparticles has been demonstrated as an efficient way to design the nanostructure of hybrid materials. In contrast to conventional inorganic fillers [8–12], POSS has the advantage of monodispersed size, low density, high thermal stability, and adjustable chemical nature. An individual unit of POSS consists of Si_8O_{12} arrayed in a cubic cage-like structure, and a variety of substituents can be linked covalently to the eight vertices around the cage. By tailoring the eight identical groups, it is possible to produce functional POSS that will undergo homopolymerization and copolymerization with other monomer to provide hybrid nanocomposites. Many POSS-containing copolymers have been synthesized in this manner, such as polysiloxane [13,14], poly(methyl methacrylate) [15], poly(4-methylstyrene) [16,17], epoxy [18,19], polynorborene [20], polyurethane [21,22], and poly(ethylene glycol) [23].

In the field of electronic devices, coating materials, bone cements etc. epoxy resins or polyimides are widely utilized as materials of supporting structures [24]. For printed circuit boards of micro-compact electronic devices, more sophisticated demands for higher thermal property materials were hardly satisfied by unmodified polymers. In particular, thermal deformation of materials must be avoided to prevent the serious destruction of devices. Epoxy resin/silica composites have been prepared by molecular level mixing of epoxy resin and silica, wherein occurs the concurrent reactions between the epoxy precursors and alkoxysilanes [25]. Silsesquioxanes bearing epoxy or amino groups were applied to the preparation of epoxy resin/silica composite materials, and successfully afford composites with high thermal properties [6].

We have investigated various organic–inorganic nanocomposites based on polyhedral oligomeric silsesquioxane (POSS) [6,23,26]. Here we report the preparation and

* Corresponding author. Tel.: +65 68741972; fax: +65 68727528.
E-mail address: jc-huang@imre.a-star.edu.sg (J. Huang).

0032-3861/$ - see front matter © 2005 Elsevier Ltd. All rights reserved.
doi:10.1016/j.polymer.2005.05.150

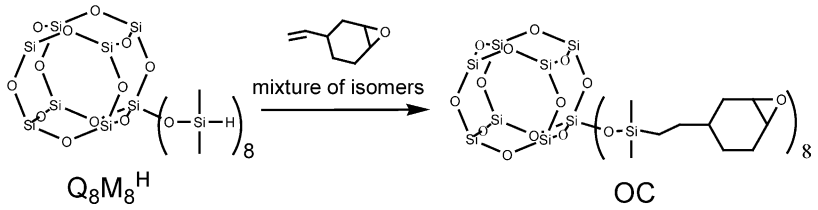

Scheme 1. Synthesis and chemical structure of OC.

characterization of novel organic–inorganic systems from polyimide and POSS epoxy. A poly(amic acid) with terminal amine groups was used instead of traditional epoxy hardeners, octa(ethylcyclohexylepoxidedimethylsiloxy) silsesquioxane (OC) was substituted for the traditional epoxy components to improve thermomechanical properties of the resulting nanocomposites. Solid-state ^{29}Si NMR data show that the thermomechanical properties of the nanocomposites are systemically adjustable. As evidenced by DMA results, some of the resulting nanocomposites were found to lose glass transition temperature due to the organic–inorganic networks of high cross-linking density.

2. Experimental

2.1. Materials

4,4′-Diaminodiphenylmethane (DADPM), 4,4′-(hexafluoroisopropylidene)-diphthalic anhydride (6F-DA), and 4-vinyl-1-cyclohexene 1,2-epoxide were purchased from Aldrich. Platinum divinyltetramethyldisiloxane complex, Pt(dvs) was obtained from Aldrich, and diluted into a 2 mM solution in anhydrous toluene. Anhydrous grade *N*-methyl-2-pyrrolidinone (NMP) was purified by distillation under a nitrogen atmosphere and dried over molecular sieves. Octa(dimethylsiloxy) silsesquioxane ($Q_8M_8^H$, Scheme 1) was provided by Hybrid Plastics. Other chemicals were used as purchased unless mentioned.

2.2. Instrumentation

Dynamic mechanical analysis (DMA) measurements were performed using a TA Instruments DMA 2980, the size of film samples is 5 mm wide and 30 mm long, and a heating rate of 3 °C/min and a frequency of 1 Hz were used. Thermomechanical analyses (TMA) were performed using a TA Instruments TMA 2940 at a heating rate of 3 °C/min. The thermal stabilities were characterized using a TGA 2050 thermogravimetric analyzer of TA Instruments at a heating rate of 20 °C/min. All the thermal analysis experiments were conducted in a dynamic nitrogen atmosphere at a flow rate of 90 ml/min.

Nanoindentation measurement was done using an UMIS-2000 Nano-indenter (Australian Scientific Instruments) with a Berkovich indenter (three-faced pyramid diamond). The load and depth of penetration were independently measured by two LVDT (linear variable differential transformer) sensors. The indentation procedure performed on all samples was as following: Load to 5 mN as the maximum load with a constant strain rate (0.05 s^{-1} in present test), hold for 60 s at the maximum load, and then unloading in the same rate to 2% of the maximum load. At least 10 indents were made on each specimen. Averaged hardness and modulus values are presented.

^{1}H NMR spectra were collected on a Bruker 400 spectrometer using chloroform-*d* as the solvent and tetramethylsilane as the internal standard. Solid-state ^{29}Si NMR spectra were also recorded on the Bruker 400 spectrometer with the frequency of 79.5 MHz. FTIR spectra were recorded on a Perkin–Elmer SPECTRUM-2000 FTIR spectrophotometer. Electrospray Ionization Mass Spectrometry (ESI-MS) was carried out on a Finnigan TSQ 7000 triple stage quadropole mass spectrometer by positive electrospray ionization.

The nanocomposite structure was imaged using a Philips CM300 FEG transmission electron microscope (TEM). Samples for the TEM experiments were prepared by burying the nanocomposite films in the epoxy capsules and curing at room temperature for 24 h. The cured epoxy samples were microtomed using a diamond knife on a Leica Ultracut, and the thin slice (90 nm) was placed on mesh 200 carbon coated copper grid for TEM observation. TEM was operated at an acceleration voltage of 300 kV.

Molecular weight and polydispersity of OC were measured on a Waters 2690 GPC system, equipped with a Waters 410 RI detector. The system was calibrated using

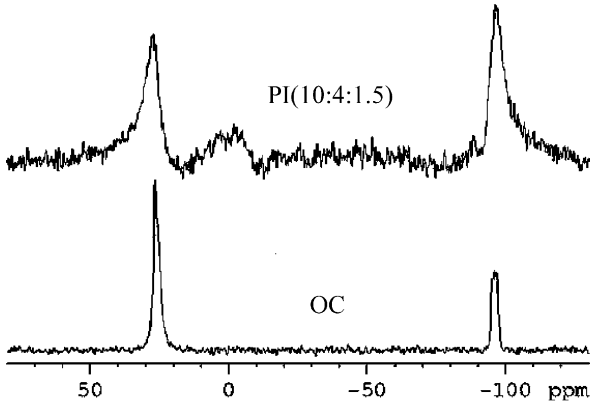

Fig. 1. Solid-state ^{29}Si NMR spectra of OC and the nanocomposite PI(10:4:1.5).

Table 1
Formulation of nanocomposites from OC

Sample	M[a]	N[b]	OC wt%[c]	DADPM (mmol)	6F-DA (mmol)	OC (mmol)	T_g (°C)
Neat PI	1		0	10 (1.983 g)	10 (4.443 g)	0 (0 g)	308.1
PI(10:6:0.5)[d]	0.6	2	17.8	10 (1.983 g)	6 (2.666 g)	0.5(1.006 g)	390.1
PI(10:6:1.5)	0.6	2/3	39.4	10 (1.983 g)	6 (2.666 g)	1.5(3.017 g)	~400
PI(10:6:2)	0.6	1/2	46.4	10 (1.983 g)	6 (2.666 g)	2(4.022 g)	388.0
PI(10:9:0.25)	0.9	1	7.8	10 (1.983 g)	9 (3.998 g)	0.25 (0.503 g)	317.8
PI(10:8:0.5)	0.8	1	15.4	10 (1.983 g)	8 (3.554 g)	0.5 (1.006 g)	344.3
PI(10:6:1)	0.6	1	30.2	10 (1.983 g)	6 (2.666 g)	1 (2.011 g)	>400
PI(10:4:1.5)	0.4	1	44.5	10 (1.983 g)	4 (1.777 g)	1.5 (3.017 g)	>400
PI(10:10:0.25)	1	0	7.3	10 (1.983 g)	10 (4.443 g)	0.25(0.503 g)	313.3
PI(10:10:0.5)	1	0	13.5	10 (1.983 g)	10 (4.443 g)	0.5(1.006 g)	320.5
PI(10:10:1)	1	0	23.8	10 (1.983 g)	10 (4.443 g)	1 (2.011 g)	318.9
PI(10:10:1.5)	1	0	31.9	10 (1.983 g)	10 (4.443 g)	1.5(3.017 g)	319.0

[a] M is the anhydride/amine mole ratio.
[b] N is the molar ratio of excess amine groups in DADPM to epoxide groups of OC.
[c] OC is octa(ethylcyclohexylepoxidedimethylsiloxy) silsesquioxane and its weight percent was calculated theoretically.
[d] The molar ratio of diamine:dianhydride:OC is 10:6:0.5.

polystyrene standards, and use THF as the eluent at a flow rate of 1.0 ml/min.

2.3. OC synthesis

Octa(ethylcyclohexylepoxidedimethylsiloxy) silsesquioxane (OC, Scheme 1) were synthesized following the previous literature with some modification [27,28]. $Q_8M_8^H$ (5 g, 4.9 mmol), anhydrous toluene (~20 ml) and 4-vinyl-1,2-cyclohexene-epoxide (9.7 g, 78.4 mmol) were charged into a flask with a reflux condenser and a magnetic stirrer. The flask was evacuated and refilled by nitrogen three times. Pt(dvs) (0.6 ml, 2 mM) was added as a catalyst, and the solution was heated at 110 °C until the resonance of Si–H bonds (about 4.7 ppm) disappeared in ^{1}H NMR spectrum. The excess starting reagents and the solvent were removed by using a rotary evaporator at 50 °C, and the product was dried at 50 °C under vacuum for 3 days. The white flakes were obtained (yield: 80%). ^{1}H NMR ($CDCl_3$, ppm): 0.15($(CH_3)_2Si$), 0.55($(CH_3)_2SiCH_2$), 3.14(CH epoxide); solid-state ^{29}Si NMR spectrum (Fig. 1, ppm): 26.0(OSi$(CH_3)_2$), −96.9(Si cube); ESI-MS (m/z): 2034.4 (found), 2034.4 (calculated) for $Si_{16}C_{80}H_{152}O_{28}Na^+$; Anal. calcd for $Si_{16}C_{80}H_{152}O_{28}$: C, 47.77, H, 7.62. Found: C, 47.68, H, 7.90; gel permeation chromatography (GPC) data: solvent THF, M_n 1717, M_w 1853, and PDI 1.07.

2.4. Preparation of nanocomposites

The compositions of the nanocomposite samples are listed in Table 1. The fixed amount of 4,4′-diaminodiphenyl methane (DADPM) and 4,4′-(hexafluoroisopropylidene)-diphthalic anhydride (6F-DA) were dissolved separately in 25 ml of *N*-methylpyrrolidinone (NMP). The two monomer solutions were mixed in a three-neck flask that has been purged with nitrogen gas to remove moisture. The mixture was stirred under N_2 at room temperature for 6 h, and a viscous polyamic acid (PAA) solution was obtained. To this

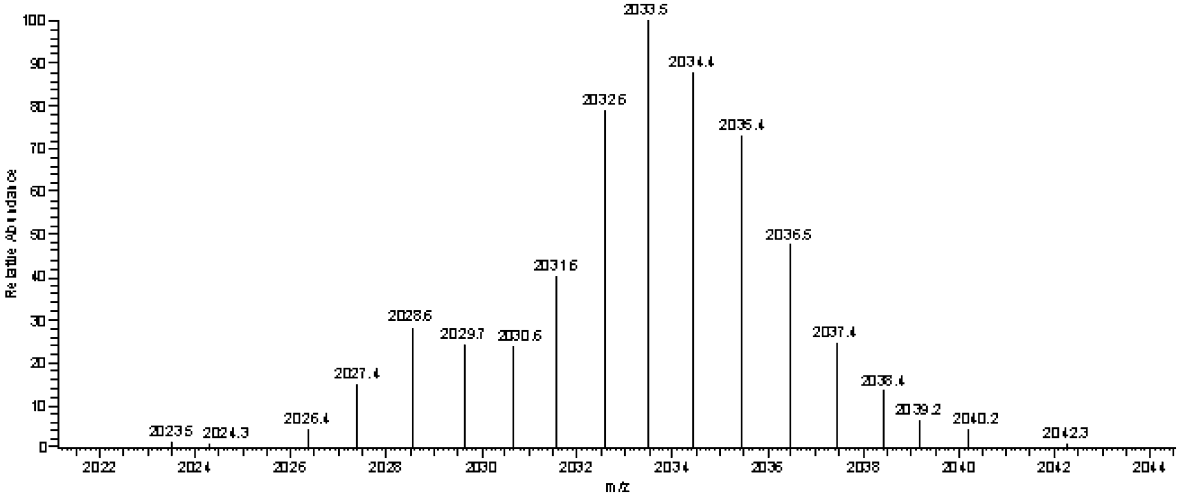

Fig. 2. Cation electrospray mass spectrum of OC in methanol.

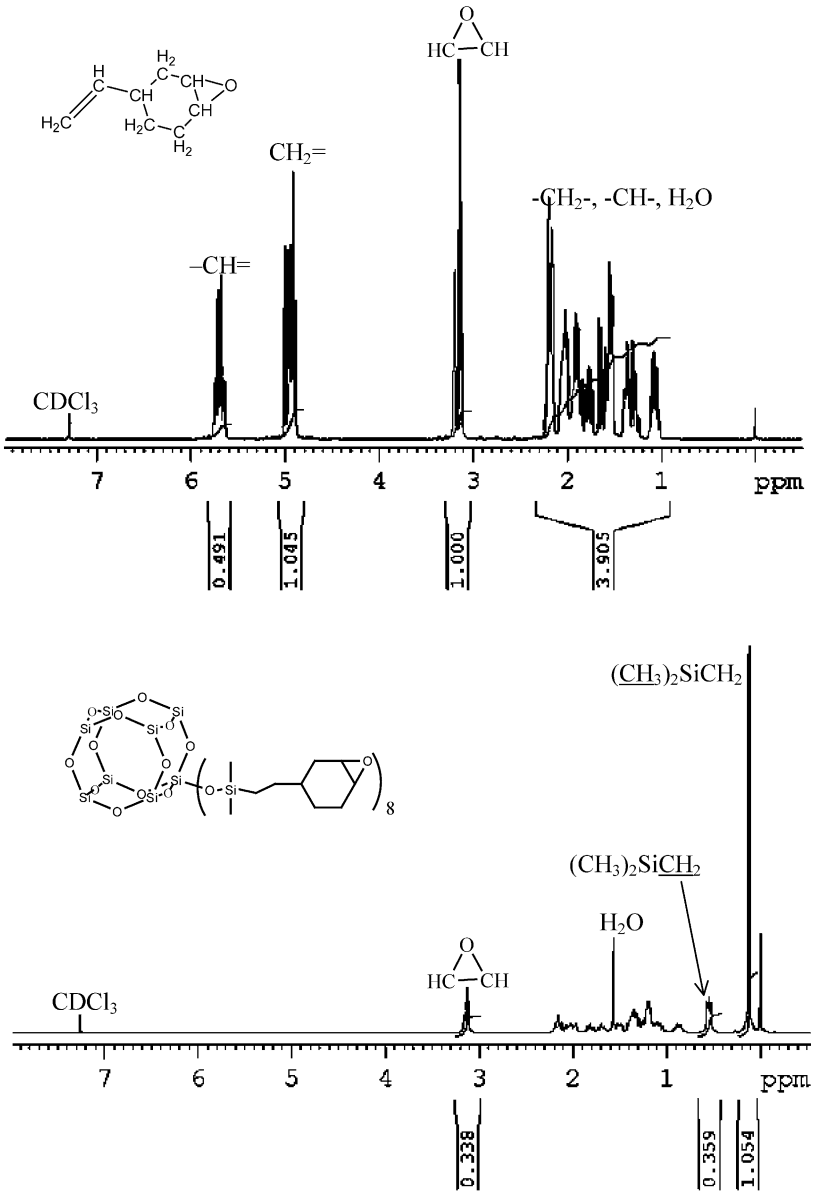

Fig. 3. ^{1}H NMR spectra of 4-vinyl-1-cyclohexene-1,2-epoxide and octa(ethylcyclohexylepoxidedimethylsiloxy) silsesquioxane (OC).

PAA solution, a pre-determined amount of OC/NMP solution was added. The mixture was stirred at room temperature for additional 2 h to give a transparent solution. The solution was then cast on a glass substrate and thermally treated at 80 °C for 8 h, 200 °C for 2 h, and 300 °C for 2 h. The films were removed from the glass substrates with the aid of deionized water, and dried at 100 °C in a vacuum oven. The films of about 50 μm thick were finally obtained.

3. Results and discussion

3.1. Preparation of nanocomposites

OC monomer was synthesized and its structure was also confirmed by ^{29}Si NMR, ^{1}H NMR, ESI-MS, elemental analyses, and GPC data. The peaks at −96.9 and 26.0 ppm in solid-state ^{29}Si NMR spectrum of OC (Fig. 1) correspond to two silicon environments in the cubic structure and its grafting groups, respectively. ESI-MS (Fig. 2) confirm the structure of OC, one cation peak was observed corresponding to $[Si_{16}C_{80}H_{152}O_{28}Na]^{+}$ (m/z = 2034.4), ESI-MS, elemental analyses, and integral data of ^{1}H NMR spectrum (Fig. 3) reveal that OC molecules have eight identical functional groups. As shown from GPC data the narrow polydispersity indicates the intact cubic cage structure with eight identical functional groups. Compared with their theoretical molecular weights the measured molecular weights of OC are smaller, because OC molecules of spherical structures show smaller hydrodynamic volume than the polystyrene standards of equivalent molecular weights [5].

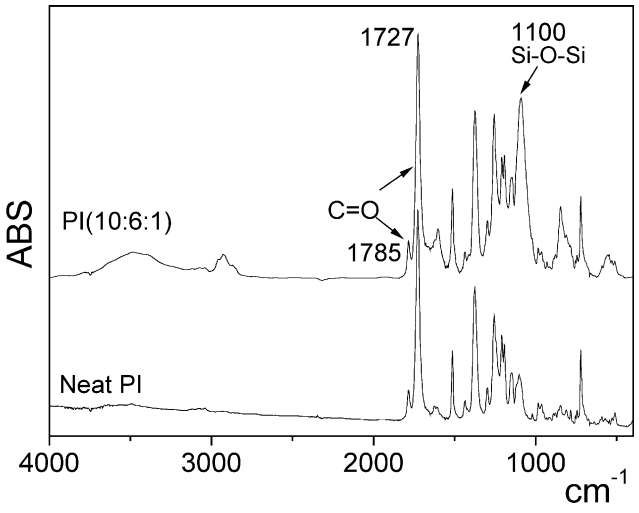

Fig. 4. FTIR spectra of the neat polyimide and the nanocomposites PI(10:6:1).

Here the neat polyimide and the nanocomposites were prepared by reaction of diamine, carboxylic dianhydride and OC. Fig. 4 shows the FTIR spectra of the neat polyimide and the nanocomposites PI(10:6:1). A complete imidized structure was confirmed by the absorption bands at 1785 cm^{-1} (asymmetric νC=O in imide groups), 1727 cm^{-1} (symmetric νC=O in imide groups), and the absence of the bands at $\sim$1660 cm^{-1} (νC=O in amide structures) and $\sim$1550 cm^{-1} (νC–N in amide structures) [6,29,30]. The absorption band of POSS was observed at 1100 cm^{-1} (asymmetric νSi–O–Si), and the epoxy components of the nanocomposites show the νO–H band at 3300–3500 cm^{-1} and the aliphatic νC–H band at 2850–3000 cm^{-1}.

The retention of the OC cubic structure in nanocomposites was directly confirmed by solid-state ^{29}Si NMR spectra as exhibited in the Fig. 1. To our knowledge, in solid-state nanocomposites the direct characterization of the silsesquioxane structures was seldom reported. Solid-state ^{29}Si NMR spectrum of the nanocomposite shows a peak at about −96.9 ppm (Fig. 1), indicating the intact cubic structure. Compared with ^{29}Si NMR spectrum of the pure OC, one additional broad peak was observed at about 0 ppm, because a part of linkages between OC and polyimide broke during the process of curing and imidization (Scheme 2). As estimated from solid ^{29}Si NMR spectrum, about 20% linkages broke. The linkages break due to the thermal imidization was also confirmed by our other experiments that will be published elsewhere. As shown in Fig. 5, the nanocomposites were modified by OH instead of OC, wherein the percentage of broken linkages between polyimide and OH is higher than that of OC due to poor thermal stability of OH grafting groups. OAPS modified nanocomposites show perfect thermal stability, no broken linkage was observed in nanocomposites (Fig. 6). The grafting groups of POSS can be varied in a systematic manner. Thermal and mechanical properties of interphase, in turn, bulk properties of composite materials can be investigated systematically. In a sequence of OAPS, OC and OH, the flexibility increases, while the thermal stability decreases. Likewise, the macroscopic properties of their modified nanocomposites change accordingly.

3.2. Thermomechanical analysis (DMA)

As shown in Table 1, the effect of two variables M and N were investigated in the preparation of the nanocomposites from OC. The ratio M is the molar ratio of anhydride groups to amine groups; the ratio N is the molar ratio of excess amine groups in DADPM to the epoxide groups in OC.

DMA analyses of the nanocomposites from OC are shown in Fig. 7(a) and Table 1. At first, in these systems the ratio M was kept at 0.6, the ratio N changed from 2 to 1/2. $M<1$ means that more diamine was added in the system, the poly(amic acid) molecules were terminated by amine groups, which could react with the epoxide groups from OC. The system of PI(10:6:1) ($M=0.6$, $N=1$) gave the highest glass transition temperature of >400 °C and comparatively high storage modulus. Additionally, as the loading of OC increased in the systems, film formability became worse, and at high OC loading the resulting films tended to fracture because of the volume shrinkage during the curing and imidization process. Therefore, in consideration of film formability, glass transition temperature and

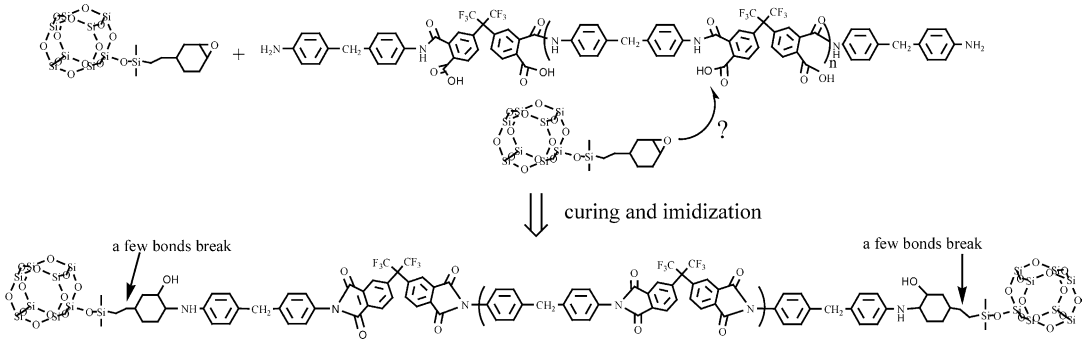

Scheme 2. Reaction of OC with poly(amic acid) to form nanocomposite.

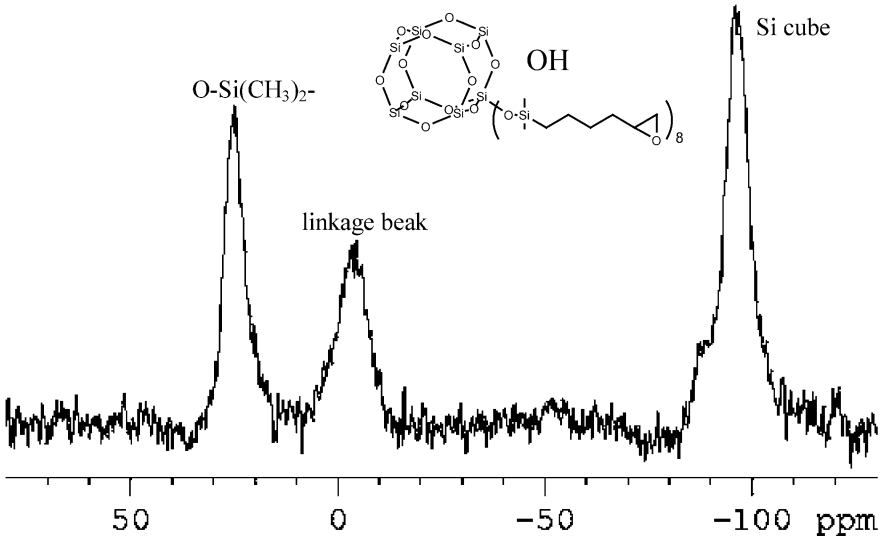

Fig. 5. Solid-state ^{29}Si NMR spectra of the polyimide nanocomposites from OH. In the formulation of this nanocomposite, the molar ratio of diamine:dianhydride:OH is 10:4:1.5.

storage modulus, the systems of molar ratio $N=1$ were selected for the further studies.

The ratio N was kept at 1, and the ratio M varied in the range from 1 to 0.4. As evidenced by DMA results (Fig. 7(b)), the variable M, the OC loading in nanocomposites, has a significant effect on glass transition temperatures and rubbery state moduli of these nanocomposites. In these profiles, the glass transition temperatures and rubbery state moduli provide the valuable information on the cross-linking densities and the nano-tether structure of the nanocomposites. As shown in the Fig. 7(b), when the ratio M decreases from 1 to 0.4, the tan δ peak of each nanocomposite shifts to higher temperature significantly, weakens, and broadens, while rubbery storage modulus increases obviously. As compared to the neat polyimide, the nanocomposite ($M=$ 0.4) shows maximum increase in T_g (>100 °C increase) and the highest rubbery state modulus of 1045.6 MPa at 400 °C ($\sim$23 times of modulus of the pristine polyimide at its T_g). It was noticed that as the ratio M decreases from 0.8 to 0.4 the nanocomposites do not show a sudden change in storage modulus upon heating, suggesting that the conventional relaxation motion of the polymer chain is highly restrained due to the high cross-linking density.

In the above systems, poly(amic acid) worked as a high molecular weight curing agent, leading to the possible epoxy curing reaction with the amide and carboxyl groups on the backbone of the PAA (Scheme 2) [31]. DMA analyses of these curing behaviors were presented in the Fig. 7(c). In contrast to the nanocomposite compositions in Fig. 7(a) and (b), the nanocomposite compositions in

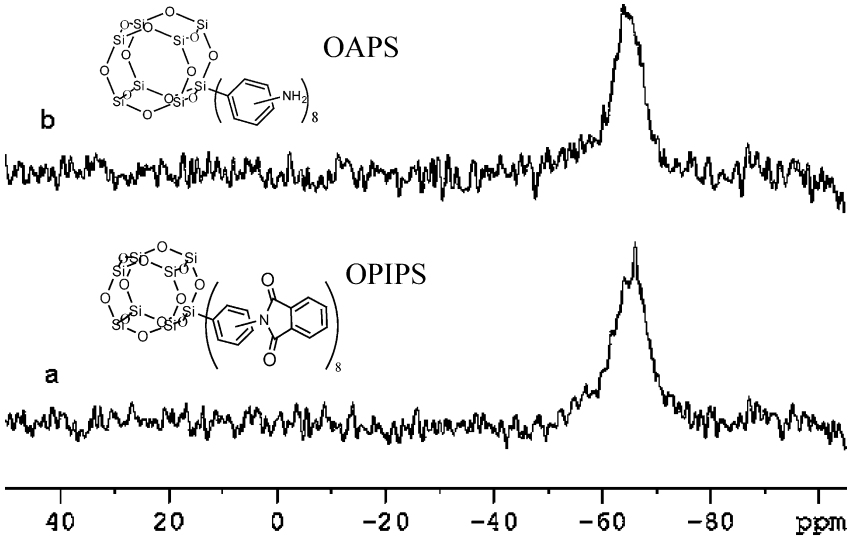

Fig. 6. Solid-state ^{29}Si NMR spectra of OPIPS (a) and the polyimide nanocomposites from OAPS (b). In the formulation of this nanocomposite, the molar ratio of diamine:dianhydride:OAPS is 4:10:1.5.

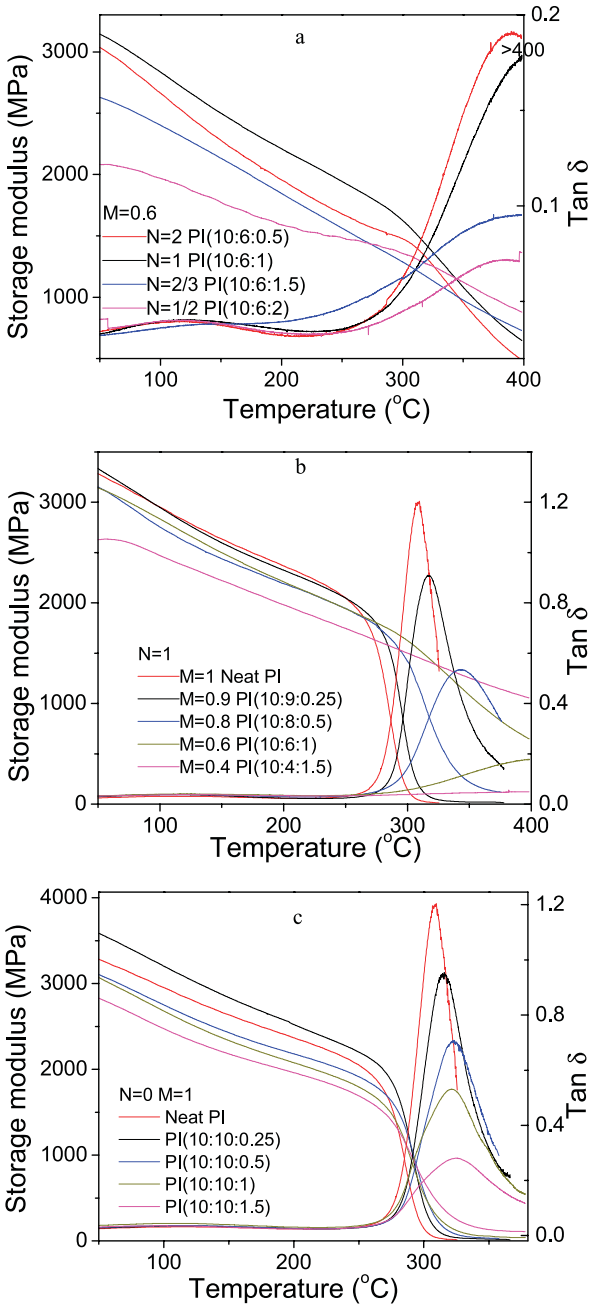

Fig. 7. DMA curves of the neat polyimide and the nanocomposites from OC.

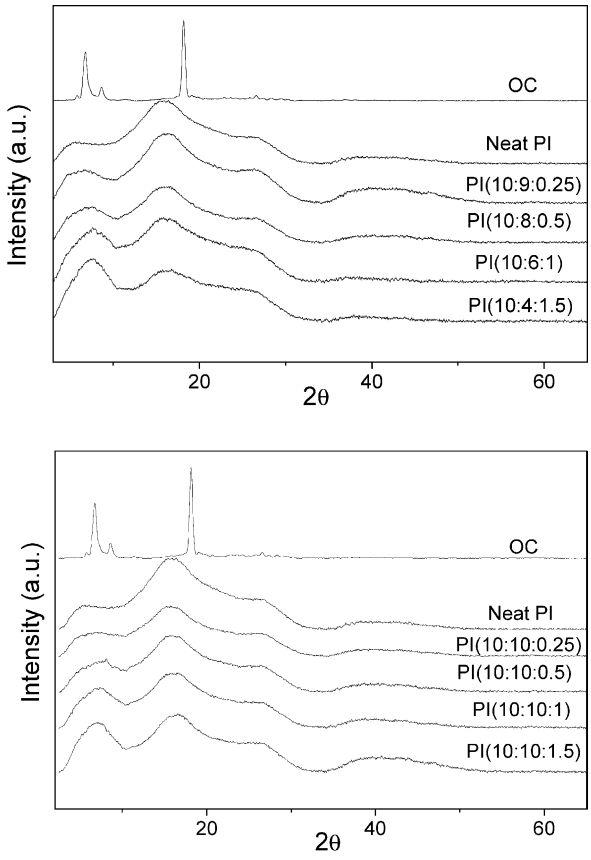

Fig. 8. XRD patterns of OC, the neat polyimide, and the nanocomposites from OC.

Fig. 7(c) were different ($M=1$, $N=0$). The equal number of diamine monomer and dianhydride monomer were added in the system, and additional OC was added in the system that might react with the amide and carboxyl groups of PAA. In the system of equivalent diamine and dianhydride the effect of the terminal amine groups could be neglected.

From Fig. 7(c), the nanocomposites from OC do not exhibit much improved dynamic mechanical behaviors. Compared with the neat polyimide the maximum increase in T_g of the nanocomposite PI(10:10:1.5) is only 12 °C, and the rubbery state moduli of the nanocomposites increase slightly. This suggests that the amide and carboxyl groups on the chain of PAA are not able to react effectively with the epoxide groups of OC, the increase in cross-linking densities of the nanocomposites is quite limited. As a consequence, the network of the nanocomposites is mainly formed by the curing reaction between the epoxide groups of POSS molecules and the terminal amine groups of polyimide molecules.

3.3. Morphology

The wide-angle X-ray patterns of the nanocomposites were shown in Fig. 8. For comparison, the X-ray patterns of OC and the neat polyimide were also shown. OC shows the diffractions at 2θs of 6.74° (101, 13.1 Å), 8.62° (110, 10.2 Å), 18.14° (330, 4.88 Å), corresponding to the diffraction of rhombohedral crystal structure [32,33]. The XRD patterns of all the polyimide nanocomposites are similar to that of the neat polyimide, except that the intensity of the diffraction at about $2\theta=7.0°$ increases as the loading of OC in nanocomposites increases, suggesting that the OC molecules tend to slightly aggregate at high OC concentration. It is also notable that the other sharp diffraction of OC at $2\theta=18.14°$ was hardly observed in the XRD patterns of the

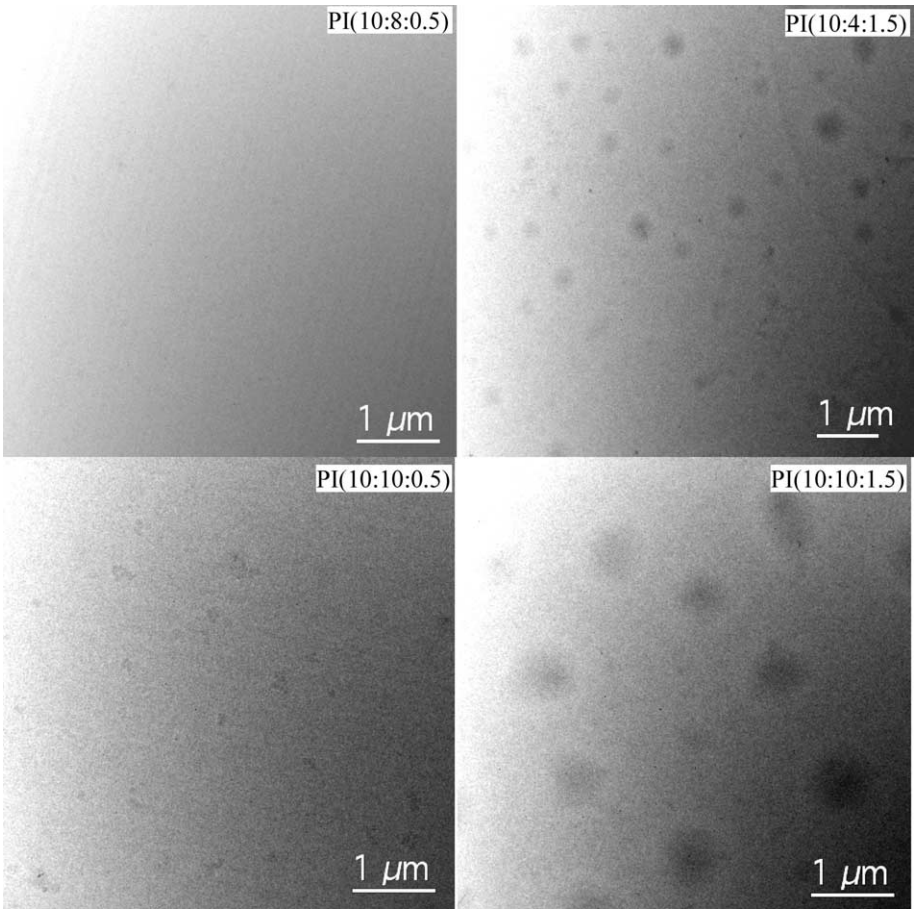

Fig. 9. TEM images of the nanocomposites from OC.

nanocomposites, because the OC molecules aggregate anisotropically in nanocomposites [34].

The above results were also confirmed by the TEM images (Fig. 9) of the nanocomposites. At high OC loading in nanocomposites, TEM images of the nanocomposite of PI(10:4:1.5) and PI(10:10:1.5) show many dark spots with size of about 400 nm, which are the domains rich in OC molecules. The polyimide components are also present in these domains, the OC molecules, therefore, aggregate in a loose manner. At low OC loading in nanocomposites, TEM image of the nanocomposite of PI(10:8:0.5) does not display any dark spots, indicating that the OC molecules are homogeneously dispersed in the nanocomposites. However, TEM image of the nanocomposite PI(10:10:0.5) displays a limited amount of small dark spots (about 70 nm), because in the systems of equal mole of diamine and dianhydride, OC molecules did not react fully with PAA, and they were more likely to aggregate.

3.4. Thermal properties

As noted above, the nanocomposites of $N=1$ (Table 1) show a significant improvement in the thermomechanical properties, this series of nanocomposites were, therefore, selected for further investigations.

Fig. 10 and Table 2 show TGA plots of the

Table 2
Thermal and mechanical properties of the nanocomposites from OC

Sample	M[a]	N[b]	T_d (°C)	CTE (ppm/K)	Young's modulus (GPa)	Elongation at break (%)	Max. stress (MPa)
Neat PI	1		513.5	55.2	2.09±0.06	6±1.2	85.2±6.3
PI(10:9:0.25)[c]	0.9	1	508.2	55.8	2.15±0.07	10±1.5	126.5±7.5
PI(10:8:0.5)	0.8	1	503.4	56.7	2.79±0.09	7±1.2	115.6±8.2
PI(10:6:1)	0.6	1	488.7	58.4	2.33±0.05	5±1	75.4±5.7
PI(10:4:1.5)	0.4	1	475.9	58.6	2.02±0.04	2±1	30.1±2.3

[a] M is the anhydride/amine mole ratio.
[b] N is the molar ratio of excess amine groups in DADPM to epoxide groups in OC.
[c] The molar ratio of diamine:dianhydride:OC is 10:9:0.25.

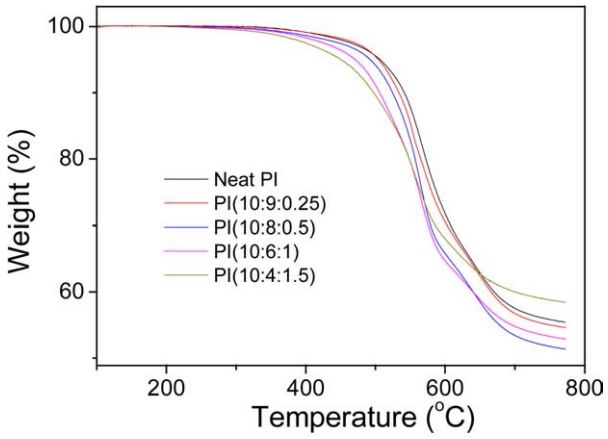

Fig. 10. TGA curves of the nanocomposites from OC.

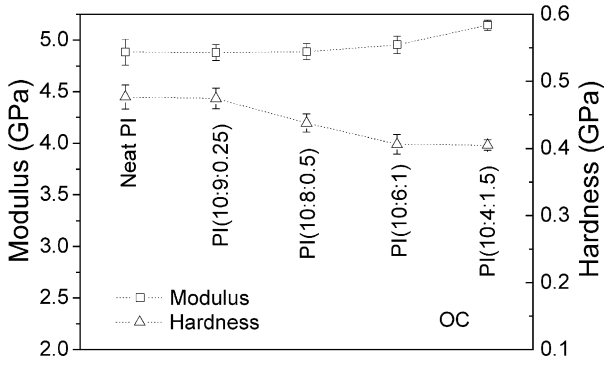

Fig. 11. Hardness and out-of-plane compressive moduli of the neat polyimide and the nanocomposites from OC as measured by nanoindentation.

nanocomposites and their on-set decomposition temperatures (T_d) respectively. The on-set decomposition temperatures (T_d) of the nanocomposites decrease continuously as the loading of OC increases. This is likely due to the poor thermal stability of aliphatic groups around OC molecules, which has been confirmed by the results of solid-state ^{29}Si NMR. The early decomposition of aliphatic linkage between OC molecules and polyimide chains will lead to the destruction of the whole network of nanocomposites.

As shown in Table 2, coefficients of thermal expansion (CTE) of the nanocomposites were measured in the temperature range between 50 and 250 °C. Although the cross-linking densities in the nanocomposites increase with the increasing OC loading, CTEs of the nanocomposites increase slightly rather than decrease, because the flexible grafting groups form a large amount of soft interphase around the OC molecules in the nanocomposites, and the soft interphase gives rise to high CTE. The previous results in our report showed that POSS molecules with higher rigidity, such as octa(aminophenyl)silsesquioxane [6], will lead to the nanocomposites of lower CTEs than the neat polyimide. From the above comparison, it was generally believed that the POSS modified hybrid materials offer an effective way to systemically adjust thermal and mechanical properties of the polymer matrices.

3.5. Mechanical properties

Mechanical properties of the nanocomposites of $N=1$ (Table 1) are shown in Table 2. As the loading of OC increases to 7.8 wt%, Tensile strength and elongation at break of the nanocomposites increase by 48 and 66% as compared to the neat polyimide. As the loading of OC was further increased, elongation at break and tensile strength both decrease. The strength and the toughness of the nanocomposites are dependent on the cross-linking density, in an appropriate range of the cross-linking density, the cross-links display the strengthening and toughening effects. Modulus of the nanocomposites shows a maximum value of 2.79 GPa at the loading of 15.4 wt% OC. The increase and decrease in the loading of OC lead to the reduction in modulus. This observation is different from our previous report [6], because the effect of the soft interphase formed by the flexible grafting groups is in competition with the effect of the increasing cross-linking densities in nanocomposites.

Fig. 11 shows the nanoindentation hardness and out-of-plane compressive moduli of the neat polyimide and the nanocomposites, a modest change in hardness and out-of-plane moduli is observed as the loading of POSS increases. The incorporation of OC in nanocomposites leads to high cross-linking density in the nanocomposites, and should result in high modulus and hardness. However, it is somewhat surprising to observe that as the loading of OC increases hardness decreases slightly, while out-of-plane compressive modulus increases slightly. The modest change in hardness and out-of-plane compressive modulus are likely originated from the effect of the soft interphase around the OC molecules, which counteracts the effect of the increasing cross-linking density.

4. Conclusions

In the preparation of the organic–inorganic nanocomposites, the reactive PAA with amine as end groups and POSS with epoxide as grafting groups were used. The curing reaction between the terminal amine groups of PAA and the epoxide groups of POSS molecules formed the linkages between POSS and polyimide molecules primarily. Solid-state ^{29}Si NMR results reveal that as the linkage structure is varied systemically, the properties of the nanocomposite interphase will change accordingly. As evidenced by the DMA data the cross-linking densities of the nanocomposites increase significantly, leading to T_g loss nanocomposite. However, the increasing cross-linking density and the soft interphase around OC molecules have opposite effects on

the properties of the nanocomposites, their effects on thermal and mechanical properties of the nanocomposites were studied.

Acknowledgements

The authors express their thanks to DSO National Lab of Singapore and Institute of Materials Research and Engineering for financially supporting this work.

References

[1] Waddon AJ, Zheng L, Farris RJ, Coughlin EB. Nano Lett 2002;2:1149–55.
[2] Leu CM, Reddy GM, Wei KH, Shu CF. Chem Mater 2003;15:2261–5.
[3] Zheng L, Farris RJ, Coughlin EB. Macromolecules 2001;34:8034–9.
[4] Choi J, Kim SG, Laine RM. Macromolecules 2004;37:99–109.
[5] Choi J, Yee AF, Laine RM. Macromolecules 2003;36:5666–82.
[6] Huang JC, He CB, Xiao Y, Mya KY, Dai J, Siow YP. Polymer 2003;44:4491–9.
[7] Mantz RA, Jones PF, Chaffee KP, Lichtenhan JD, Gilman JW, Ismail IMK, et al. Chem Mater 1996;8:1250–9.
[8] Zhu ZK, Yin J, Cao F, Shang XY, Lu QH. Adv Mater 2000;12:1055–7.
[9] Huang JC, Zhu ZK, Yin J, Qian XF, Sun YY. Polymer 2001;42:873–7.
[10] Huang JC, Zhu ZK, Yin J, Zhang DM, Qian XF. J Appl Polym Sci 2001;79:794–800.
[11] Huang JC, Zhu ZK, Ma XD, Qian XF, Yin J. J Mater Sci 2001;36:871–7.
[12] Giannelis EP. Adv Mater 1996;8:29.
[13] Lichtenhan JD, Vu NQ, Carter JA, Gillman JW, Feher FJ. Macromolecules 1993;26:2141–2.
[14] Shockey EG, Bolf AG, Jones PF, Schwab JJ, Chaffee KP, Haddad TS, et al. Appl Organomet Chem 1999;13:311–27.
[15] Lichtenhan JD, Otonari YA, Carr MJ. Macromolecules 1995;28:8435–7.
[16] Haddad TS, Lichtenhan JD. Macromolecules 1996;29:7302–4.
[17] Romo-Uribe A, Mather PT, Haddad TS, Lichtenhan JD. J Polym Sci, Part B: Polym Phys 1998;36:1857–72.
[18] Lee A, Lichtenhan JD. Macromolecules 1998;31:4970–4.
[19] Lee A, Lichtenhan JD. J Appl Polym Sci 1999;73:1993–2001.
[20] Mather PT, Jeon HG, Romo-Uribe A, Haddad TS, Lichtenhan JD. Macromolecules 1999;32:1194–203.
[21] Hsiao BS, White H, Rafailovich M, Mather PT, Jeon HG, Phillips S, et al. Polymer 2000;49:437–40.
[22] Fu BX, Hsiao BS, Pagola S, Stephens P, White H, Rafailovich M, et al. Polymer 2001;42:599–611.
[23] Huang JC, Li X, Lin TT, He CB, Xiao Y, Mya KY, et al. J Polym Sci, Part B: Polym Phys 2004;42:1173–80.
[24] Fujiwara M, Kojima K, Tanaka Y, Nomura R. J Mater Chem 2004;14:1195–202.
[25] Ochi M, Takahashi R. J Polym Sci, Part B: Polym Phys 2001;39:1071.
[26] Huang JC, Lim PC, Shen L, Pallathadk PK, Zeng K, He C. Acta Mater 2005;53:2395–404.
[27] Laine RM, Choi J, Lee I. Adv Mater 2001;13:800–3.
[28] Crivello JV, Malik R. J Polym Sci, Part A: Polym Chem 1997;35:407–25.
[29] Feger G, Khojasteh MM, McGrath JE. Polyimides: materials, chemistry and characterization. Amsterdam: Elsevier; 1989.
[30] Mittal KL. Polyimides: synthesis, characterization and applications. New York: Plenum Press; 1984.
[31] Gaw K, Kikei M, Kakimoto M, Imai Y. React Funct Polym 1996;30:85–91.
[32] Waddon AJ, Coughlin EB. Chem Mater 2003;15:4555–61.
[33] Brown JF, Voft LH, Prescott PI. J Am Chem Soc 1963;86:1120–5.
[34] Zheng L, Waddon AJ, Farris RJ, Coughlin EB. Macromolecules 2002;35:2375–9.